Theoretical analysis of extrusion of rectangular, hexagonal and octagonal composite clad rods

C.W. Wu, R.Q. Hsu*

Department of Mechanical Engineering, National Chiao Tung University, 1001 Ta-Hsueh Road, 300, Hsinchu, Taiwan

Abstract

Composite clad rods with non-axisymmetric cross-sectional areas are commercially important owing to their extensive industrial applications such as in electrodes, conductors and chemical devices. For instance, in the processing of superconductor wire, increasing the packing density involves closely packing superconductor rods which have a hexagonal cross-section next to each other inside the high purity copper tube. During extrusion process, non-uniform deformation tends to occur because the core and sleeve of a composite clad rod is usually composed of materials with different mechanical properties. The first recognized paper on round-to-square drawing/extrusion with variable corner radius was presented by Boer et al. in 1979. In this study, we present a model based on upper-bound theorem to analyze the extrusion of composite clad rods with non-axisymmetric cross-section. Velocity fields for both core and sleeve are generated with the assistance of a product's cross-sectional profile functions. Products with rectangular, hexagonal and octagonal sections are chosen as the study objects. Also discussed herein are numerical results for various process variables such as semi-die angle, reduction of area, frictional condition of die, and product shape complexity. According to these results, the extrusion pressure and product dimensional change are closely related to the process variables. © 1999 Elsevier Science Ltd. All rights reserved.

Keywords: Non-axisymmetric extrusion; Composite clad rods; Upper bound; Non-uniform velocity

1. Introduction

Demands for composite clad rods, i.e. rods consisting of two or more different materials, have accelerated as their applications in diverse fields such as electronics, nuclear, and chemical have

---

* Corresponding author.

Nomenclature

r, ϕ, y	cylindrical coordinates
$R_o, R_\infty, R_f, R_{cf}$	the radius of sleeve and core before extrusion and after extrusion, respectively
Rss, Rsc	function represent die surface and core/sleeve inter-surface profiles, respectively
V_o, V_f	entrance velocity of the billet and exit velocity of extruded product, respectively
Γ_s, Γ_f	surfaces of shear velocity discontinuities and friction, respectively
$V_{rs}, V_{\phi s}, V_{ys}$	velocity components of sleeve in the cylindrical coordinates (r, ϕ, y), respectively
$V_{rc}, V_{\phi c}, V_{yc}$	velocity components of core in the cylindrical coordinates (r, ϕ, y), respectively
ω_s, ω_c	angular velocity of sleeve and core, respectively
U_s, U_c	uniform velocity component in the extrusion axis of sleeve and core, respectively
D_s, D_c	non-uniform velocity component in the extrusion axis of sleeve and core, respectively
$\partial U_s/\partial y, \partial U_c/\partial y$	first derivative of uniform velocity component in the extrusion axis of sleeve and core with respect to y, respectively
$\partial \omega_s/\partial \phi, \partial \omega_c/\partial \phi$	first derivative of angular velocity of sleeve and core with respect to ϕ, respectively
Z_s, Z_c	functions of $\beta_s, \beta_c, Rss, Rsc$, and L, respectively
$\partial Z_s/\partial y, \partial Z_c/\partial y$	first derivative of function Z_s, Z_c with respect to y, respectively
$\partial Rss/\partial y, \partial Rsc/\partial y$	first derivative of die surface and core/sleeve inter-surface profile functions with respect to y, respectively
$\phi_f(y)$	angle of geometric symmetry surface
δ, β_s, β_c	optimization parameters introduced in the velocity fields
L	die length (dimensionless)
$R_f(\phi)$	product radius function
A_s	area of sleeve at die exit
J	total power consumption in extrusion
$\dot{W}_{is}, \dot{W}_{ss}, \dot{W}_{fd}$	power dissipation due to internal deformation, internal shear of the sleeve and friction at die surface, respectively
$\dot{W}_{ic}, \dot{W}_{sc}, \dot{W}_{f1}$	power dissipation due to internal deformation, internal shear of the core and friction at core/sleeve inter-surface, respectively
$\dot{W}_i, \dot{W}_s, \dot{W}_f$	power dissipation due to internal deformation, internal shear of the sleeve and friction, respectively
V_p	volume of the plastic region
$\sigma_0, \dot{\bar{\varepsilon}}$	the yield stress and effective strain rate of materials, respectively
$\Delta V_{\Gamma_s}, \Delta V_{\Gamma_f}$	the relative slip velocity on Γ_s and Γ_f surfaces, respectively
P_{avg}	average extrusion pressure
α	semi-die angle
Yss, Ysc	yield stress of the sleeve and core, respectively
RA	reduction of area of billet
m, m_1	friction factor at the die surface and core/sleeve inter-surface, respectively

expanded. Among typical examples of composite clad rods include commercially available super-conductor cables which have NbTi or NbSn as cores and pure copper as an outer sleeve. Composite clad rods are usually made by extruding an assembled core/sleeve billet, in which their cross-section profile can be round or any arbitrary shape. Owing to the differences in mechanical properties of core and sleeve, a composite clad rod in extrusion occasionally encounters a non-homogeneous deformation and (in severe cases) even fracturing of the product.

Most research related to extrusion of composite clad rod, the focus being primarily on the product with an axi-symmetric cross-section. However, as applications involving non-axisymmetric composite clad rods are increasingly frequent, an analytical method must be developed to resolve the above problem.

Boer et al. first used the upper-bound method to analyse the direct drawing of square section rod from round bar [1]. Juneja and Prakash [2] obtained upper-bound loads for extrusion of polygonal sections by utilizing a conventional spherical velocity field. However, their analysis was limited to products with polygonal sections. Nagpal and Altan [3] proposed dual stream functions to obtain a kinematically admissible velocity field that demonstrated a three-dimensional metal flow. Their model, however was confined to the extrusion of ellipse bar or rod. Yang and Lee [4] adopted a conformal mapping approach to obtain a velocity field for extrusion through concave and convex-shaped dies where geometrical similarity is preserved through out the deformation. The axial velocity in their study was kept uniform at any cross-section. Yang et al. [5] also analyzed the extrusion of a helical bar from cylindrical billet with linear converging dies. All the research objects for the above-mentioned studies are solid bars composed of only one material. Kiuchi [6] proposed an analytical model to extrude a composite clad rod through arbitrarily shaped dies. However, the velocity distributions in the axial direction were assumed to be uniform through out the deformation process. This is not an ideal situation for most extrusion processes.

In this study, we employ the upper-bound method, as well as a three-dimensional velocity field which has a non-uniform velocity distribution along the extrusion axis and a non-linear variation velocity component along the radius to extrude a composite rod. All the three-dimensional velocity fields of sleeve and core were generated with the aid of the shape of the final product. Composite rod billets with non-axisymmetric cross-sectional profiles like rectangular, hexagonal and octagonal sections are examined. These results are presented in the following section.

2. Formulation of velocity field

Fig. 1 schematically depicts the extrusion of a composite clad rod with an arbitrary cross-sectional profile. Owing to the complexity of the material flow in a non-axisymmetric composite rod extrusion, the following assumptions must be made to establish the analysis model:

1. The core and the sleeve are isotropic, homogeneous, and rigid-plastic materials.
2. The die is assumed to be rigid throughout the extrusion process.
3. Temperature effect is neglected in the analysis.
4. Plastic deformation is assumed to have occurred within zones bound by die entrance plane (A-A′), die exit plane (B-B′) and the die surface for both core and sleeve. Core/sleeve inter-surface is determined by the deformation characteristics. In the undeformed region, composite rod
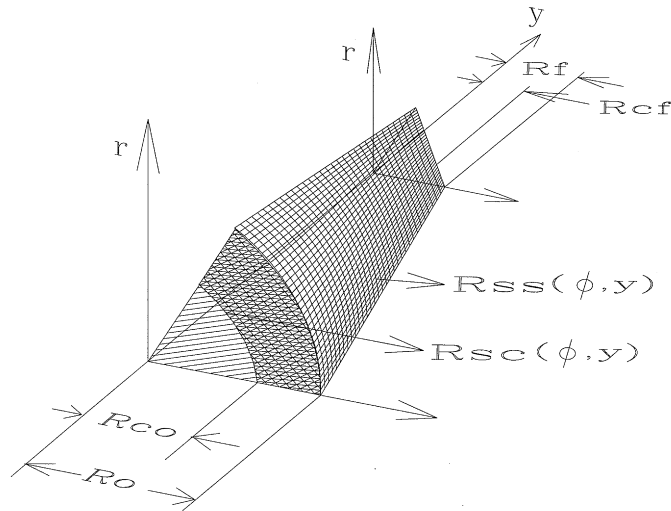
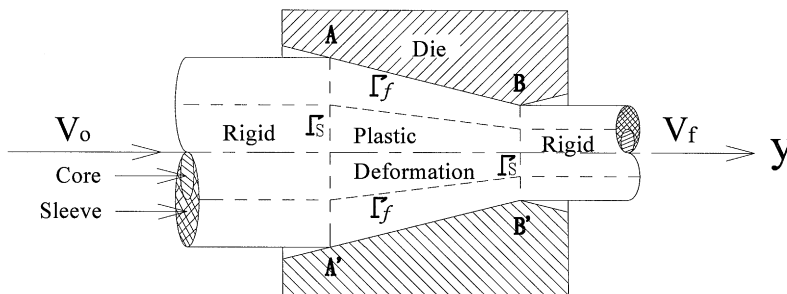Fig. 1. Schematic representation of extrusion of composite clad rod with a arbitrary cross-sectional profile.

Fig. 2. Plastic and rigid regions.

moves as a rigid body in the extrusion direction (y-axis) before entering the plastic deformation zone with velocity V_o, and after exit of the plastic zone with velocity V_f as indicated in Fig. 2.
5. In order to simplify the derivation of the velocity field, here, we assume the core remains circular after extrusion.

In the analysis, a constant friction factor m_1 is adopted to calculate the friction energy loss on the core/sleeve inter-surface.

Fig. 3 illustrates a composite clad rod extruded through a linear converging die. At the die entrance, both sleeve and core move with a uniform velocity component in the extrusion axis (y). After entering the plastic deformation zone, sleeve and core may experience non-uniform deformation owing to their material characteristics, thus their velocity components in the y-axis may differ from each other. If this tendency continues up to the die exit, the composite rod will no longer be a bonded sound product. While constructing an admissible velocity field, a cylindrical coordinate system (r, ϕ, y) is adopted and it is further assumed that for either sleeve or core, the rotational velocity component is linearly distributed along the radius, that is $V_{\phi s} = r\omega_s(\phi, y)$,
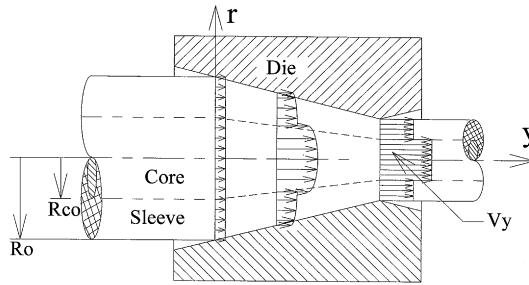
Fig. 3. Velocity components in y-axis.

$V_{\phi c} = r\omega_c(\phi, y)$. For axis-symmetric cases, however, angular velocity $\omega(\phi, y)$ is zero. The three-dimensional admissible velocity fields for core and sleeve can be derived under the condition of incompressibility of materials or a constant volume flow. These results are summarized below.

(a) *Velocity for sleeve*:

$$V_{ys}(r, \phi, y) = D_s(r, \phi, y)U_s(y), \tag{1}$$

$$V_{\phi s}(r, \phi, y) = r\omega_s(\phi, y), \tag{2}$$

$$V_{rs}(r, \phi, y) = -\frac{r}{2}\left(\frac{\partial U_s(y)}{\partial y} + \frac{\partial \omega_s(\phi, y)}{\partial \phi}\right) + \frac{r^3}{4}\left(Z_s(\phi, y)\frac{\partial U_s(y)}{\partial y} + U_s(y)\frac{\partial Z_s(\phi, y)}{\partial y}\right)$$

$$-\frac{1}{r}\left\{\begin{array}{l} \dfrac{Rsc^4(\phi, y)}{4}\left[Z_s(\phi, y)\dfrac{\partial U_s(y)}{\partial y} + U_s(y)\dfrac{\partial Z_s(\phi, y)}{\partial y}\right] \\[2mm] -\dfrac{Rsc^2(\phi, y)}{2}\left[\dfrac{\partial U_s(y)}{\partial y} + \dfrac{\partial \omega_s(\phi, y)}{\partial \phi}\right] \\[2mm] -[1 - Z_s(\phi, y)Rsc^2(\phi, y)]U_s(y)Rsc(\phi, y)\dfrac{\partial Rsc(\phi, y)}{\partial y} \end{array}\right\}. \tag{3}$$

Here

$$D_s(r, \phi, y) = 1 - \frac{4\beta_s y(L - y)}{Rss^2(\phi, y)L^2}r^2 \quad Z_s(\phi, y) = \frac{4\beta_s y(L - y)}{Rss^2(\phi, y)L^2}, \tag{4}$$

$$U_s(y) = \frac{V_0 \displaystyle\int_0^{\phi_T(0)} [Rss^2(\phi, 0) - Rsc^2(\phi, 0)] \, d\phi}{\displaystyle\int_0^{\phi_T(0)} \{[Rss^2(\phi, y) - Rsc^2(\phi, y)] - Z_s(\phi, y)[[Rss^4(\phi, y) - Rsc^4(\phi, y)]/2]\} \, d\phi}, \tag{5}$$

$$\omega_s(\phi, y) = \frac{-2}{Rss^2(\phi, y) - Rsc^2(\phi, y)} \int_0^{\phi_f(y)} \begin{bmatrix} V_{ys}(Rss(\phi, y), \phi, y)Rss(\phi, y)\dfrac{\partial Rss(\phi, y)}{\partial y} \\[2mm] - V_{ys}(Rsc(\phi, y), \phi, y)Rsc(\phi, y)\dfrac{\partial Rsc(\phi, y)}{\partial y} \\[2mm] + \begin{bmatrix} \dfrac{Rss^2(\phi, y) - Rsc^2(\phi, y)}{2} \\[2mm] - Z_s(\phi, y)\dfrac{Rss^4(\phi, y) - Rsc^4(\phi, y)}{4} \end{bmatrix}\dfrac{\partial U_s(y)}{\partial y} \\[2mm] - \dfrac{Rss^4(\phi, y) - Rsc^4(\phi, y)}{4}\dfrac{\partial Z_s(\phi, y)}{\partial y}U_s(y) \end{bmatrix} \, d\phi.$$

(6)

(b) *Velocity of core*:

$$V_{yc}(r, \phi, y) = D_c(r, \phi, y)U_c(y), \tag{7}$$

$$V_{\phi c}(r, \phi, y) = r\omega_c(\phi, y), \tag{8}$$

$$V_{rc}(r, \phi, y) = -\frac{r}{2}\left[\frac{\partial U_c(y)}{\partial y} + \frac{\partial \omega_c(\phi, y)}{\partial \phi}\right] + \frac{r^3}{4}\left(Z_c(\phi, y)\frac{\partial U_c(y)}{\partial y} + U_c(y)\frac{\partial Z_c(\phi, y)}{\partial y}\right). \tag{9}$$

Here,

$$D_c(r, \phi, y) = 1 - \frac{4\beta_c y(L - y)}{Rsc^2(\phi, y)L^2}r^2 \quad Z_c(\phi, y) = \frac{4\beta_c y(L - y)}{Rsc^2(\phi, y)L^2}, \tag{10}$$

$$U_c(y) = \frac{V_0 \displaystyle\int_0^{\phi_f(0)} Rsc^2(\phi, 0)\,d\phi}{\displaystyle\int_0^{\phi_f(0)} [Rsc^2(\phi, y) - Z_c(\phi, y)Rsc^4(\phi, y)/2]\,d\phi}, \tag{11}$$

$$\omega_c(\phi, y) = -\frac{2}{Rsc^2(\phi, y)} \int_0^{\phi_f(y)} \left\{ \begin{aligned} & V_{yc}(Rsc(\phi, y), \phi, y)Rsc(\phi, y)\frac{\partial Rsc(\phi, y)}{\partial y} \\[2mm] & + \frac{Rsc^2(\phi, y)}{2}\frac{\partial U_c(y)}{\partial y} \\[2mm] & - \frac{Rsc^4(\phi, y)}{4}\left[\frac{\partial Z_c(\phi, y)}{\partial y}U_c(y) + Z_c(\phi, y)\frac{\partial U_c(\phi, y)}{\partial y}\right] \end{aligned} \right\} \, d\phi. \tag{12}$$

Herein, β_s, β_c are parameters to be explained in the following section. The die surface profile is given by function $Rss(\phi, y)$, while core/sleeve inter-surface is given by function $Rsc(\phi, y)$. In the case of linear converging die, the die surface can be expressed as

$$Rss(\phi, y) = \left\{ R_o - \left[(R_o - R_f(\phi)) \frac{y}{L} \right] \right\}. \tag{13}$$

On the other hand, a cone-shape core/sleeve inter-surface can be represented as

$$Rsc(\phi, y) = \left\{ R_{co} - \left[(R_{co} - R_{cf}) \frac{y}{L} \right] \right\}. \tag{14}$$

Herein, R_o, R_{co} denote the radii of sleeve and core, respectively, before extrusion. As the velocity fields are three-dimensional and the velocity component in extrusion axis is non-uniform, we assume the core remains circular after extrusion in order to derive conceptual velocity fields and simplify the problem. Thus, Rcf is the radius of the core after extrusion, R_f is the radius of the section corner of the sleeve (in the case of non-circular product) after extrusion and L is die length. One characteristic of this velocity field is, once the functions $Rss(\phi, y)$, $Rsc(\phi, y)$ are defined, each velocity component can be calculated directly.

3. Optimal parameters

As mentioned earlier, owing to dissimilar mechanical properties, core and sleeve may not deform homogeneously. Under this circumstance, the cross-section area ratio of core to sleeve at die exit is different from that of the assembled billet. The equivalent radius of core, Rcf, is then calculated from

$$Rcf = \left[\frac{(1 + \delta)A_s}{\pi} \right]^{1/2} \frac{R_{co}}{R_o}, \tag{15}$$

where A_s is the area of sleeve at die exit.

The value of parameter δ is determined by the minimization of total extrusion power. On the other hand, velocity distribution of sleeve and core in the extrusion axis (y), Vys, Vyc, can be thought of as composed of a uniform component, U_s, U_c and a non-uniform component, $D_s(r, \phi, y)$, $D_c(r, \phi, y)$, which again are determined by the parameters β_s, β_c.

Obviously, $Vys(r, \phi, y) = Us(y)$, $Vyc(r, \phi, y) = Uc(y)$ when $y = 0, L$. Restated, the velocity components in the y-axis for either sleeve or core in both die entrance and die exit are uniformly distributed. Only in the plastic deformation zone, $D_s(r, \phi, y)$ and $D_c(r, \phi, y)$, can a non-zero function exist. Herein, two independent parameters β_s, β_c are introduced to make this happen. In upper-bound analysis, δ, β_s, β_c are considered as optimal parameters and their values are mathematically optimized by minimizing the total power J consumed in the extrusion process.

4. Power consumption

While extruding a composite clad rod, power consumption includes the power deemed necessary to overcome the resistance to deformation of both sleeve and core, $\dot{W}_{is}\dot{W}_{ic}$; shear power losses,

$\dot{W}_{ss}, \dot{W}_{sc}$ over boundaries of velocity discontinuities (slip), A-A′, B-B′; frictional power consumed along the die surface and inter-layer surface, $\dot{W}_{fd}, \dot{W}_{f1}$. This power consumption can be estimated by integrating the strain rate and the yield stress over the entire deformation volume. Each strain rate can be readily calculated from the velocity field formulated above. Formulations for the above-mentioned power items are expressed as follows:

$$\dot{W}_i = \int_{V_p} \sigma_0 \dot{\bar{\varepsilon}} \, dv, \tag{16}$$

$$\dot{W}_s = \int_{\Gamma_s} \frac{1}{\sqrt{3}} \sigma_0 \Delta V_{\Gamma_s} \, ds, \tag{17}$$

$$\dot{W}_f = \int_{\Gamma_f} \frac{m}{\sqrt{3}} \sigma_0 \Delta V_{\Gamma_f} \, dA, \tag{18}$$

where, σ_0 denotes the yield stress of the materials, $\dot{\bar{\varepsilon}}$ represents the effective strain rate of the materials, V_p is the volume of plastic deformation region, ΔV_{Γ_s} denotes the relative slip velocity at velocity discontinuity surfaces, m represents the friction factor, and ΔV_{Γ_f} is the relative slip velocity at frictional surfaces.

5. Results and discussion

This study closely examines extrusions of rectangular, hexagonal and octagonal clad sections from round clad rods. All the dies used in the analysis are linearly connected and divided equally anglewise as shown in Fig. 4.

Herein, semi-die angles are defined as the angle of die surface inclination. As Fig. 5 depicts, the pressure deemed necessary to extrude composite hexagonal sections from round billets is shown against semi-die angles. This figure reveals that the pressure required is larger at small semi-die angles. With an increasing semi-die angle, extrusion pressure gradually decreases and then reaches a minimum. Beyond this angle, the extrusion pressure increases with an increasing semi-die angle. This tendency indicates that an optimal semi-die angle exists for the extrusion of composite clad rod. With small die angles, the length of contact between the billet and die is longer, causing significantly high friction losses. Meanwhile, with large die angles, die lengths are reduced but the
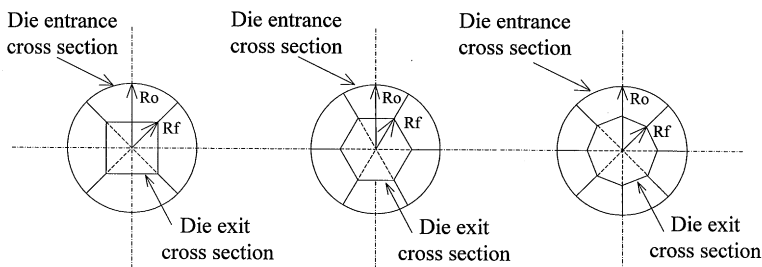

Fig. 4. Extrusion dies for rectangular, hexagonal, octagonal sections.
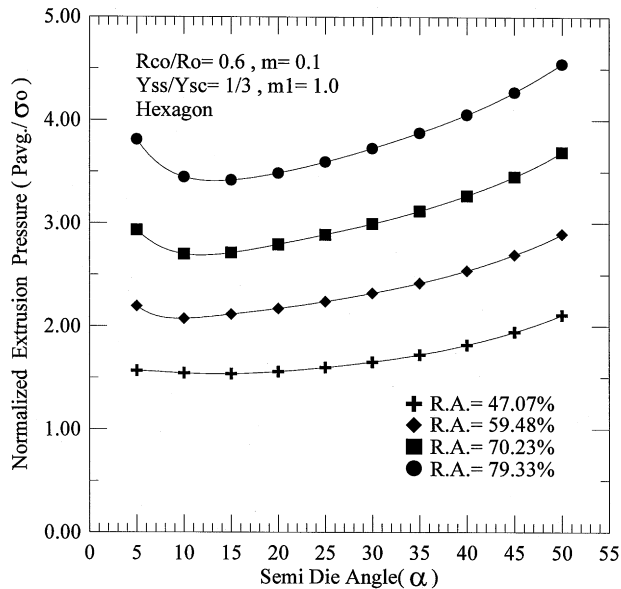
Fig. 5. Effects of semi-die angle on extrusion pressure (soft sleeve/hard core).

internal deformation becomes a predominant factor. For the working conditions shown in this figure, extrusion pressures are minimum at a semi-die angle between 10 and 20°.

For billet with a hard sleeve/soft core combination, the tendency for the variation of extrusion pressure against semi-die angle (Fig. 6) is exactly the same as for those of soft sleeve/hard core combinations in Fig. 5.

Figs. 7 and 8 depict how the semi-die angle influences the exit radius of core, Rcf. For soft sleeve/hard core combinations (Fig. 7), the yield stress of a core is larger than that of a sleeve and thus is more resistant to deformation, particularly at larger die angles where plastic flow are more severe. Therefore, the exit radius of core tends to increase with an increasing semi-die angles. On the other hand, for the hard sleeve/soft core composite clad rod combinations, the exit radius of core tends to decrease with increasing semi-die angle (Fig. 8).

Fig. 9 plots the normalized extrusion pressure against semi-die angles under three different die surface frictional conditions. This figure indicates that the normalized extrusion pressure generally increases with an increasing friction factor. For the case where the friction factor is zero, no optimal semi-die angle exists. This situation is attributed to the situation when the frictional power is zero, the total extrusion pressure consists of only the internal deformation. Fig. 10 displays parameter β_s which describes the degree of non-uniformity of velocity component Vys, against a semi-die angle. A larger positive value of β_s indicates Vys has a more prominent concavity distribution. A larger die surface friction factor implies a more sticky die surface, material flow in extrusion axis is thus retarded on the die surface, therefore, β_s is larger. For a larger semi-die angle, while other process variables remain the same, the deformation is more severe. The difference of velocity component in extrusion axis for a larger semi-die angle is larger than for a smaller semi-die angle. Thus, β_s is larger.
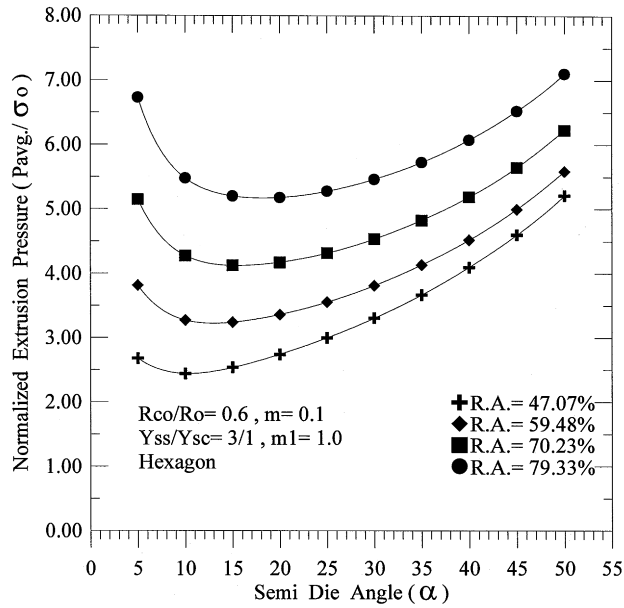
Fig. 6. Effects of semi-die angle on extrusion pressure (hard sleeve/soft core).
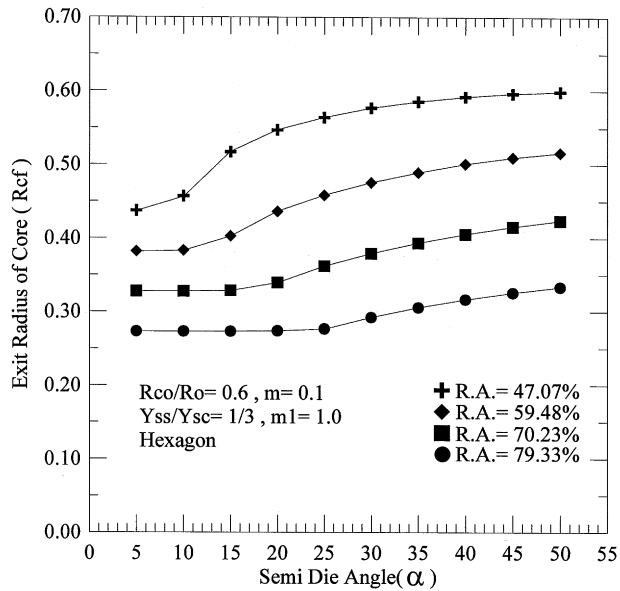

Fig. 7. Effects of semi-die angle on exit radius of core (soft sleeve/hard core).
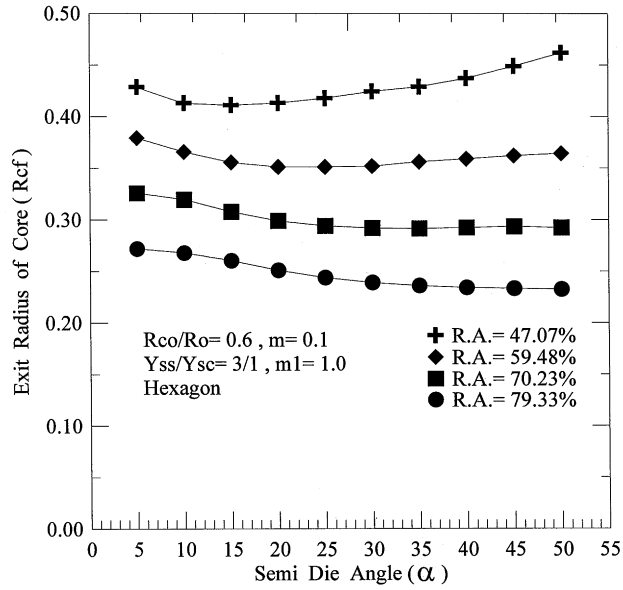
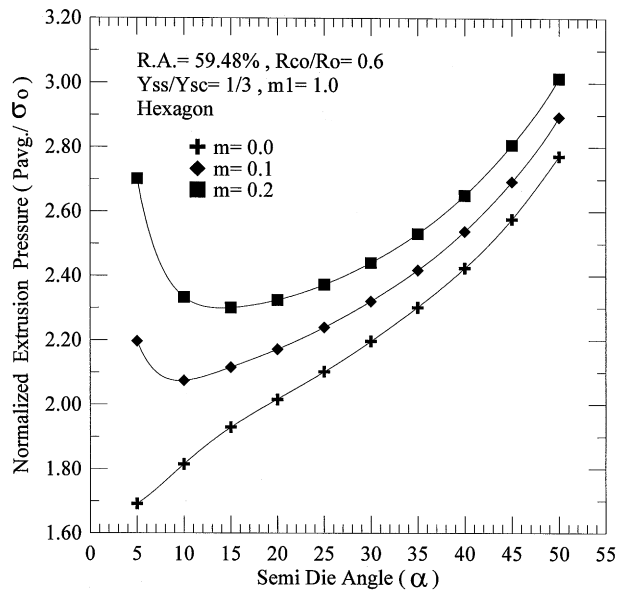Fig. 8. Effects of semi-die angle on exit radius of core (hard sleeve/soft core).

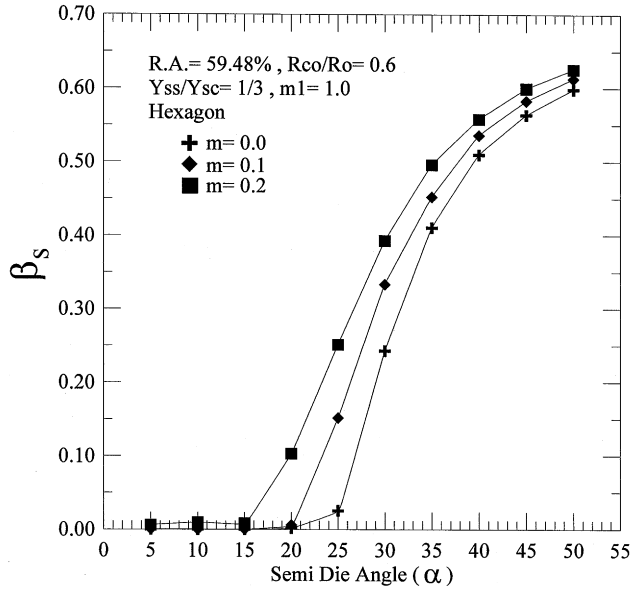Fig. 9. Effects of friction factor of die on extrusion pressure (soft sleeve/hard core).

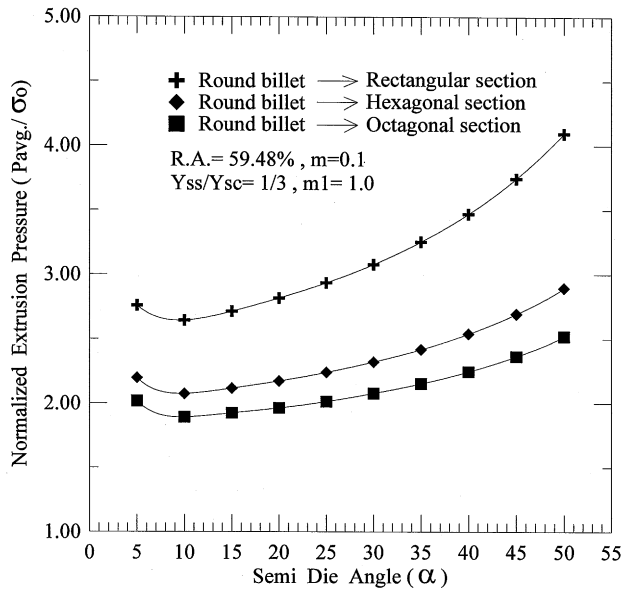Fig. 10. Effects of friction factor of die on β_s (soft sleeve/hard core).

Fig. 11. Effects of product shape on extrusion pressure (soft sleeve/hard core).
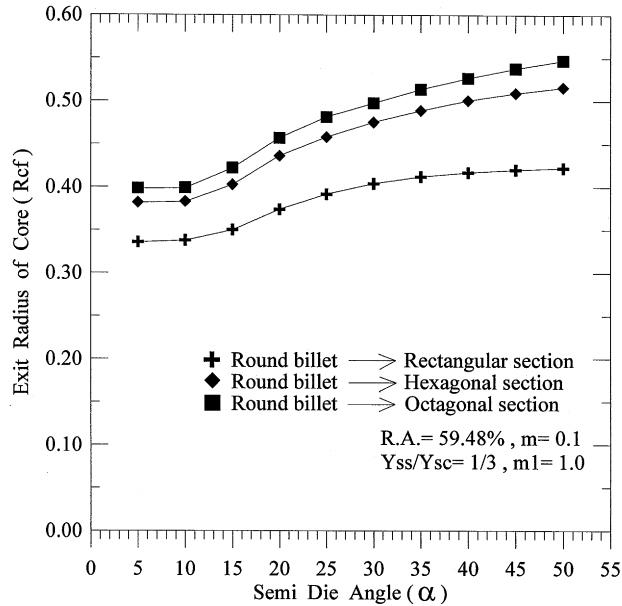
Fig. 12. Effects of product shape on exit radius of core (soft sleeve/hard core).

Fig. 11 presents the extrusion pressure for rectangular, hexagonal and octagonal composite clad sections which are extruded from round composite clad billets. From this figure, we can infer that with the same reduction ratio, rectangular section, which has the least number of sides requires the largest extrusion pressure. As the number of section sides increases, the product shape gradually approaches a round bar and the extrusion pressure reduces correspondingly. In this case, the exit radius of core increases with an increasing number of section sides, as shown in Fig. 12.

6. Conclusions

This work presents a generalized three-dimensional kinematically admissible velocity field to extrude a composite clad rod. The proposed method is then applied to the extrusion of rectangular, hexagonal and octagonal sections from a round composite billet. Also examined herein are factors that dominate the deformation pattern of the rod: semi-die angle, friction on die surface, relative strength, extrusion ratio and product shape. Based on those results, we can conclude the following:

1. For semi-die angles between 10 and 20°, the extrusion pressure required is the lowest.
2. Higher frictional losses promote non-uniform velocity distribution in the extrusion direction (β_s increase).
3. With the same amount of reduction ratio, the extrusion pressure decreases with an increasing number of the product section sides.

4. The proposed model can be applied to extrude a composite clad rod with an irregular cross-section if its cross-sectional profile can be mathematically expressed by a function.

References

[1] Boer CR, Schneider WR, Eliasson B, Avitzur B. An upper bound approach for the direct drawing of square section rod from round bar. 20th MTDR Conference, 1979, pp. 149–156.
[2] Juneja BL, Prakash R. An analysis for drawing and extrusion of polygonal sections. International Journal of Machine Tool Design and Research 1975;15:1–30.
[3] Nagpal V, Altan T. Analysis of the three-dimensional flow in extrusion of shapes with the use of dual stream functions. Proceedings of the Third North American Metalworking Research Conference, 1975, pp. 26–40.
[4] Yang DY, Lee CH. Analysis of three-dimensional extrusion of sections through curved dies by conformal transformation. International Journal of Mechanical Sciences 1978;20:541–52.
[5] Yang DY, Kim MU, Lee CH. An analysis for extrusion of helical shapes from round billets. International Journal of Mechanical Sciences 1978;20:695–705.
[6] Kiuchi M, Hsu RQ. Drawing of non-axisymmetric clad rods and wires. 4 Drawing of square, hexagonal and other non-symmetric clad rods. The Proceedings of the Japanese Spring Conference for the Technology of Plasticity, 1989, pp. 151–154.